Atmospheric
Chemistry
and Physics

Supplement of

Measurement report: Comprehensive seasonal study of the composition and sources of submicron aerosol during the JULIAC campaign in Germany

Lu Liu et al.

Correspondence to: Lu Liu (lu.liu1@psi.ch) and Thorsten Hohaus (t.hohaus@fz-juelich.de)
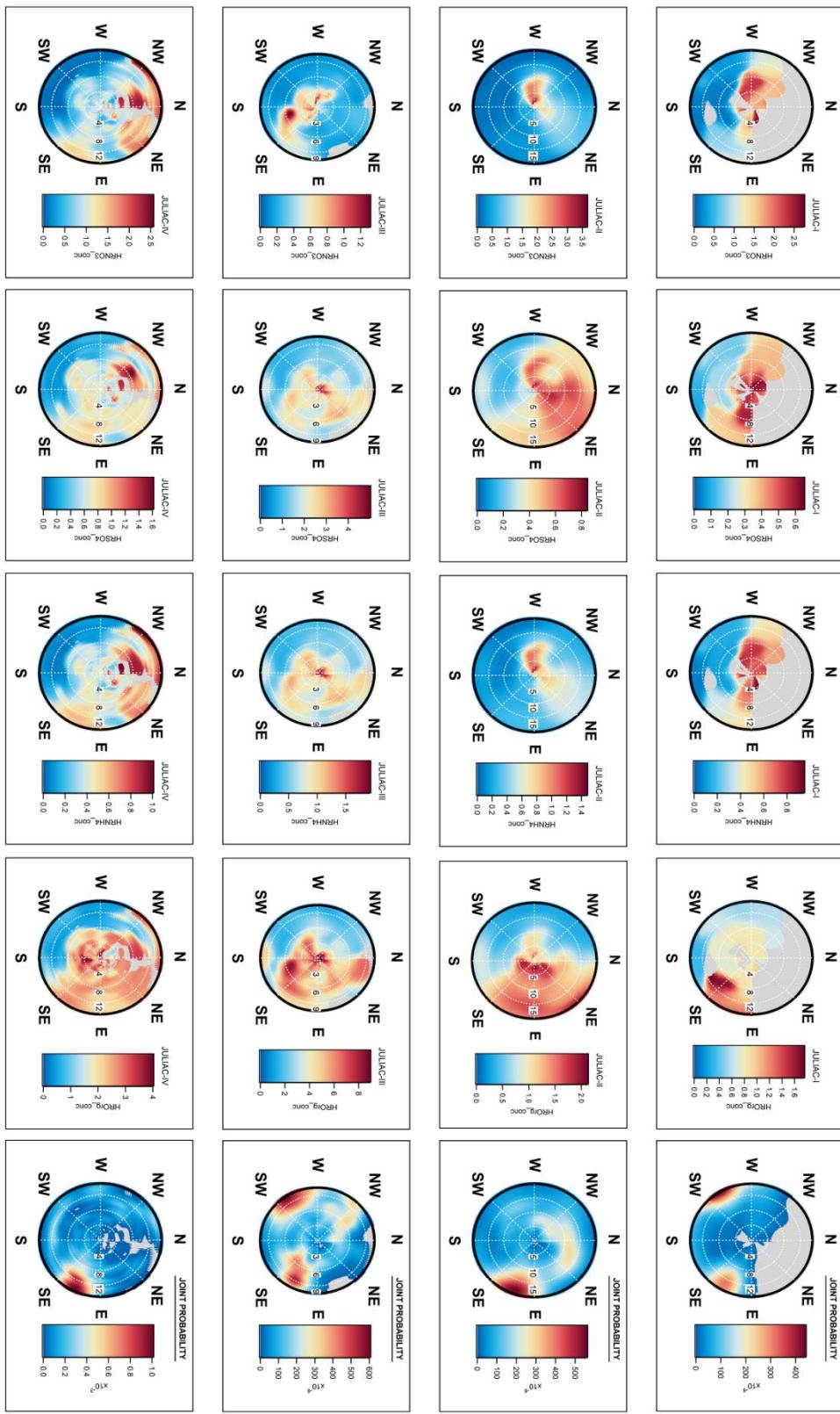
Figure S1 Polar diagrams using non-parametric wind regressions are shown for all JULIAC-intensive phases, illustrating the bulk concentrations of nitrate, sulfate, ammonium, and organics, as well as the joint probability, which captures the combined influence of wind direction and speed on the presence of all these compounds. The polar plot is based on wind direction and wind speed measured at a height of 50 meters. The concentrations of major submicron aerosol components are represented using color coding in the polar plot to indicate their potential regional influences.
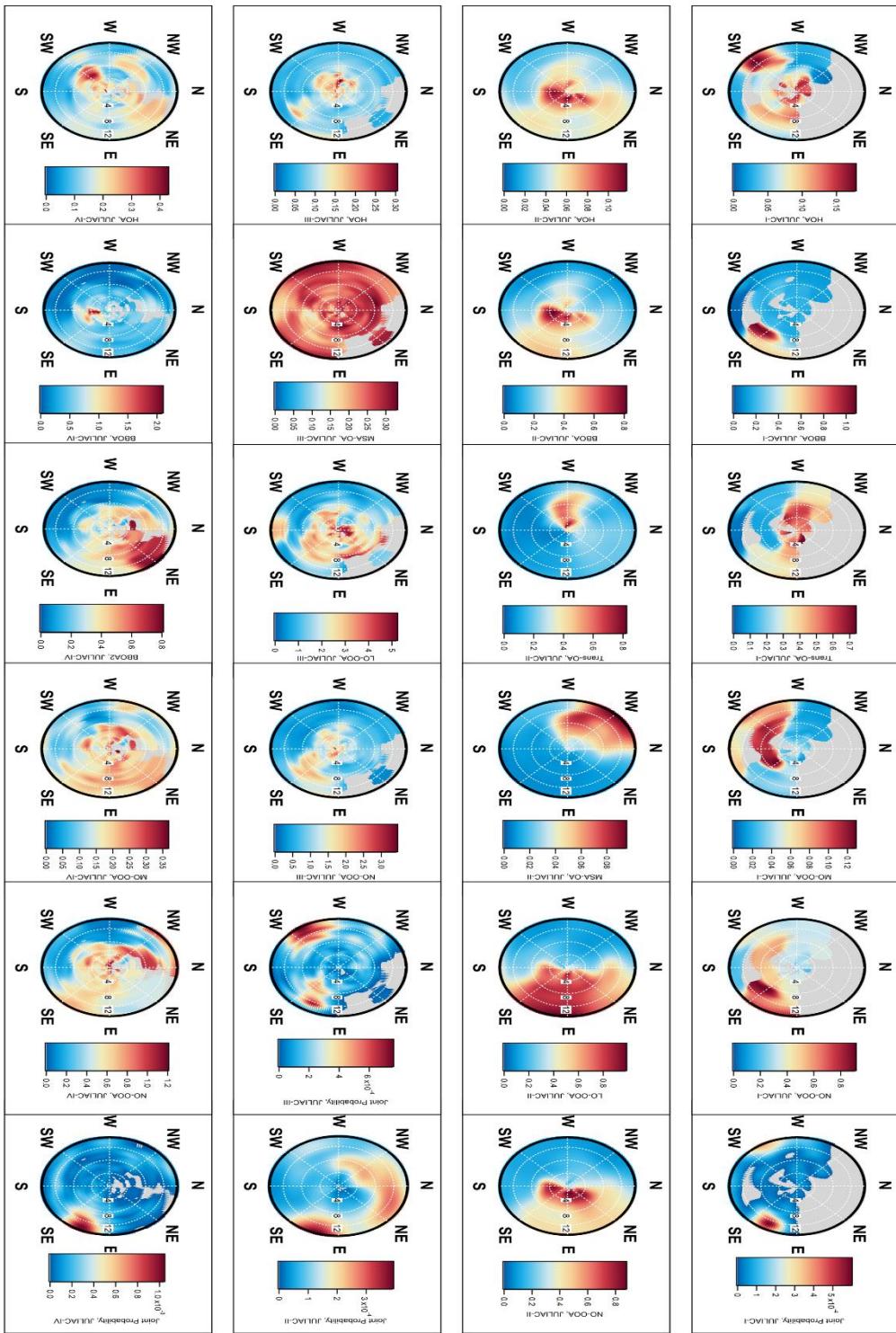
Figure S2 Polar diagrams using non-parametric wind regressions are shown for all JULIAC-intensive phases, illustrating source factors contribution as well as the joint probability, which captures the combined influence of wind direction and speed on the presence of all these compounds. The polar graph is created based on the wind direction and wind speed measured in 50-m height. The OA contribution from all OA sources are utilized as color code in the polar graph to illustrate the potential regional source.
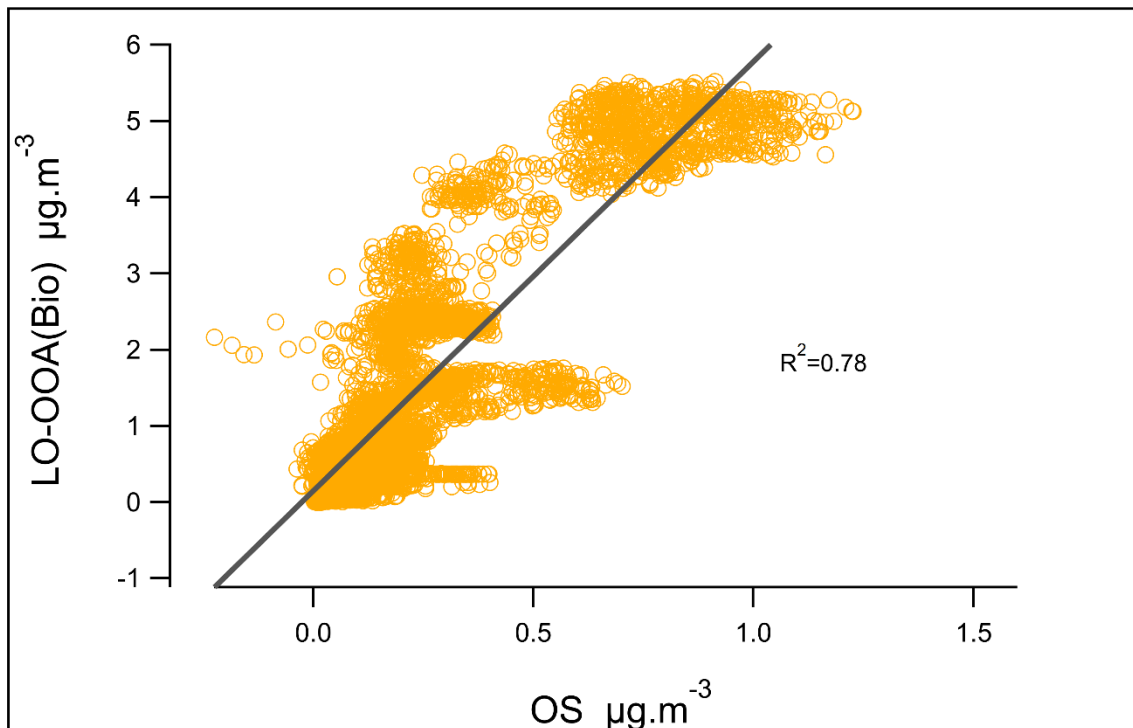
Figure S3 The correlation between the mass concentration of biogenic derived OOA, LO-OOA(Bio), and the aerosol organosulfur calculated based on AMS measurements during summer (JULIAC-III) is displayed. The linear fitting and corresponding correlation efficiency was also marked in graph.
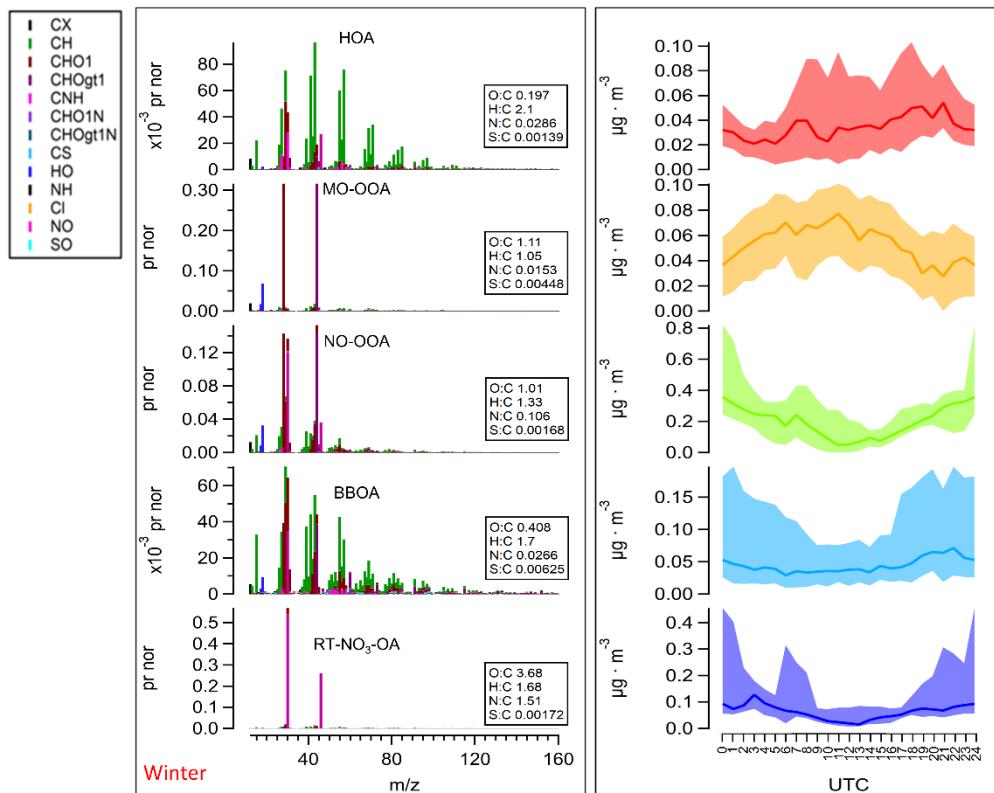
Figure S4 The results overview of source apportionment resolved by PMF analysis of aerosol nitrate and organics for the

winter of 2019. From left to right, the graph shows the variation of contribution to OA for each source factor, i.e. the

high-resolution spectra of source factors colored by the family group of ions, and the diurnal pattern of the median (solid

line) and interquartile range (IQR, shaded area) of the contribution of the corresponding source factor. The elemental ra-

tio (OM:OC, O:C, H:C) of all OA factors is shown in the graph.
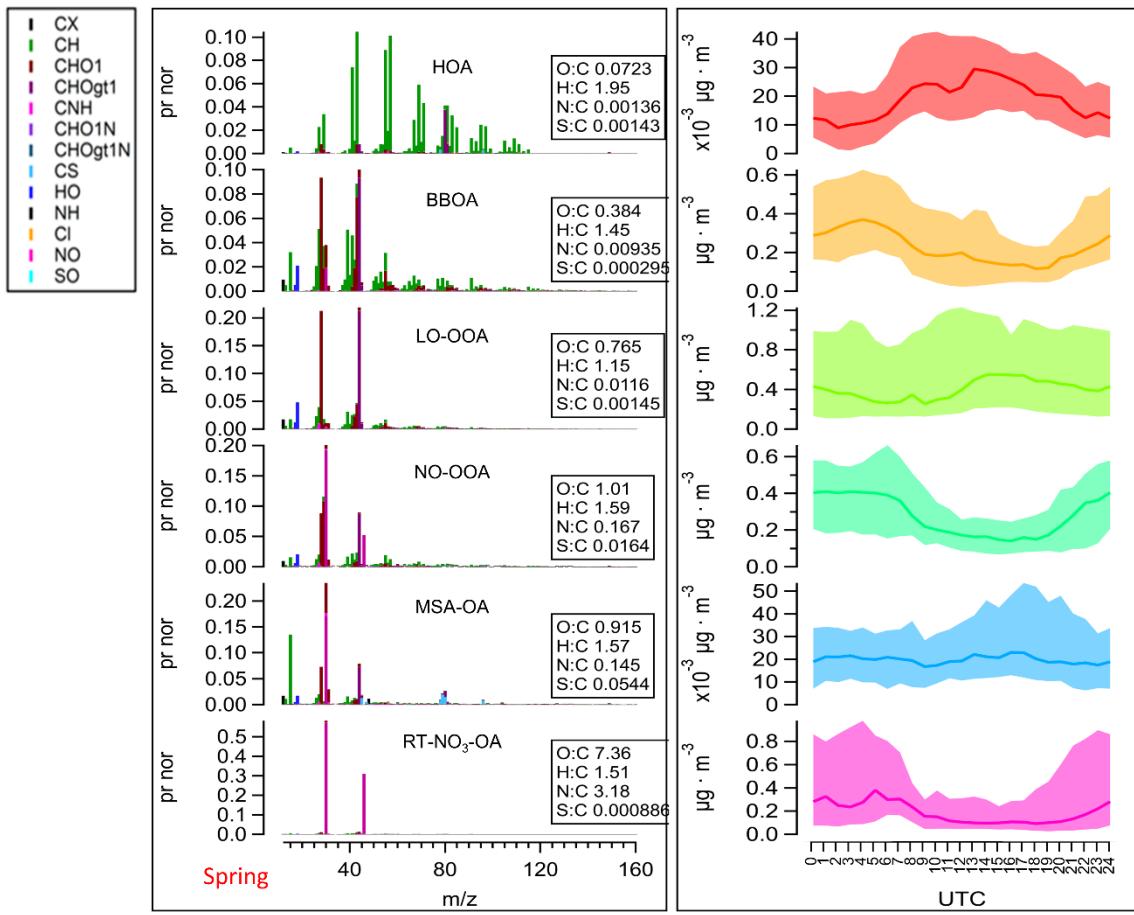
Figure S5 The results overview of source apportionment resolved by PMF analysis of aerosol nitrate and organics for the spring of 2019. From left to right, the graph shows the variation of contribution to OA for each source factor, i.e. the high-resolution spectra of source factors colored by the family group of ions, and the diurnal pattern of the median (solid line) and interquartile range (IQR, shaded area) of the contribution of the corresponding source factor. The elemental ratio (OM:OC, O:C, H:C) of all OA factors is shown in the graph.
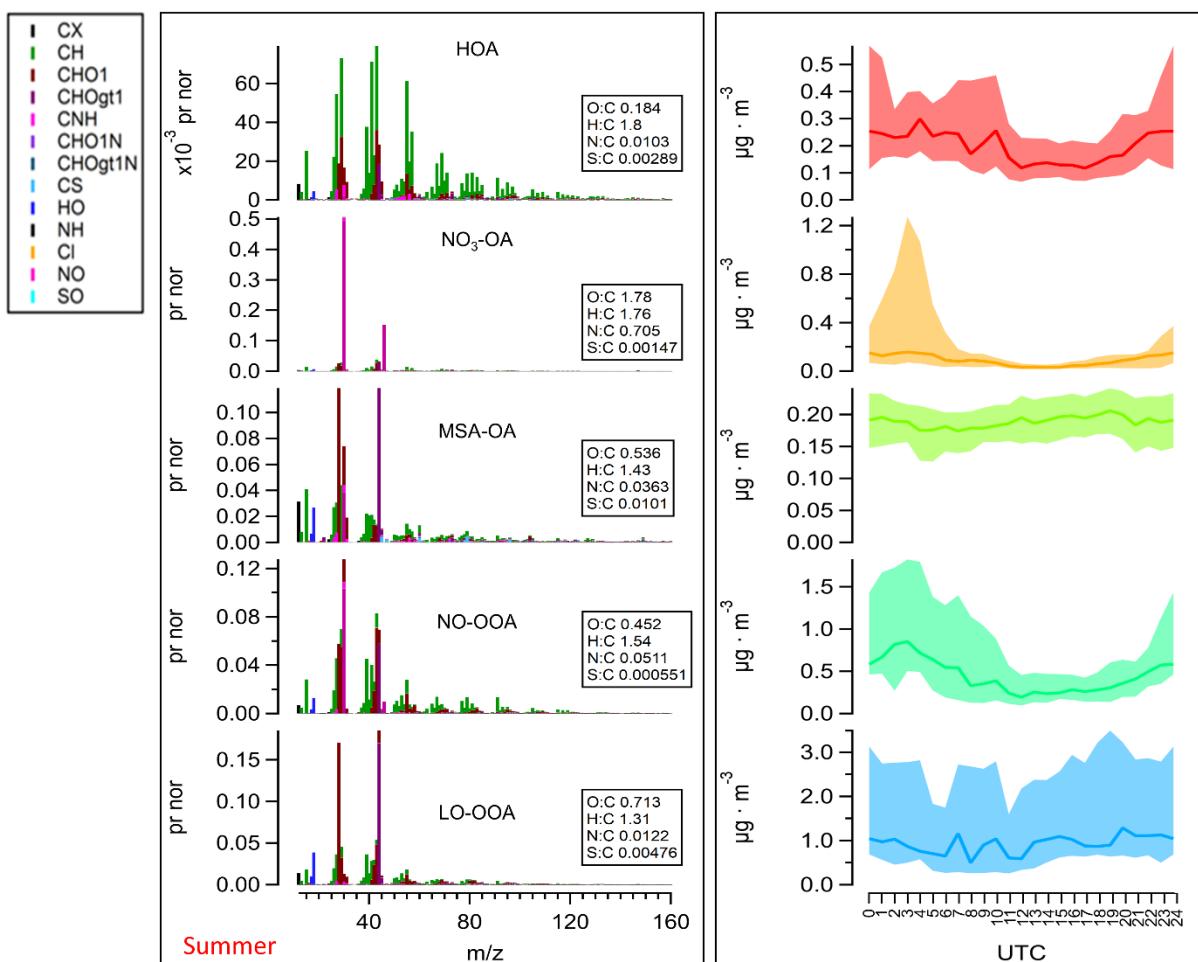
Figure S6 The results overview of source apportionment resolved by PMF analysis of aerosol nitrate and organics for the summer of 2019. From left to right, the graph shows the variation of contribution to OA for each source factor, i.e. the high-resolution spectra of source factors colored by the family group of ions, and the diurnal pattern of the median (solid line) and interquartile range (IQR, shaded area) of the contribution of the corresponding source factor. The elemental ratio (OM:OC, O:C, H:C) of all OA factors is shown in the graph.
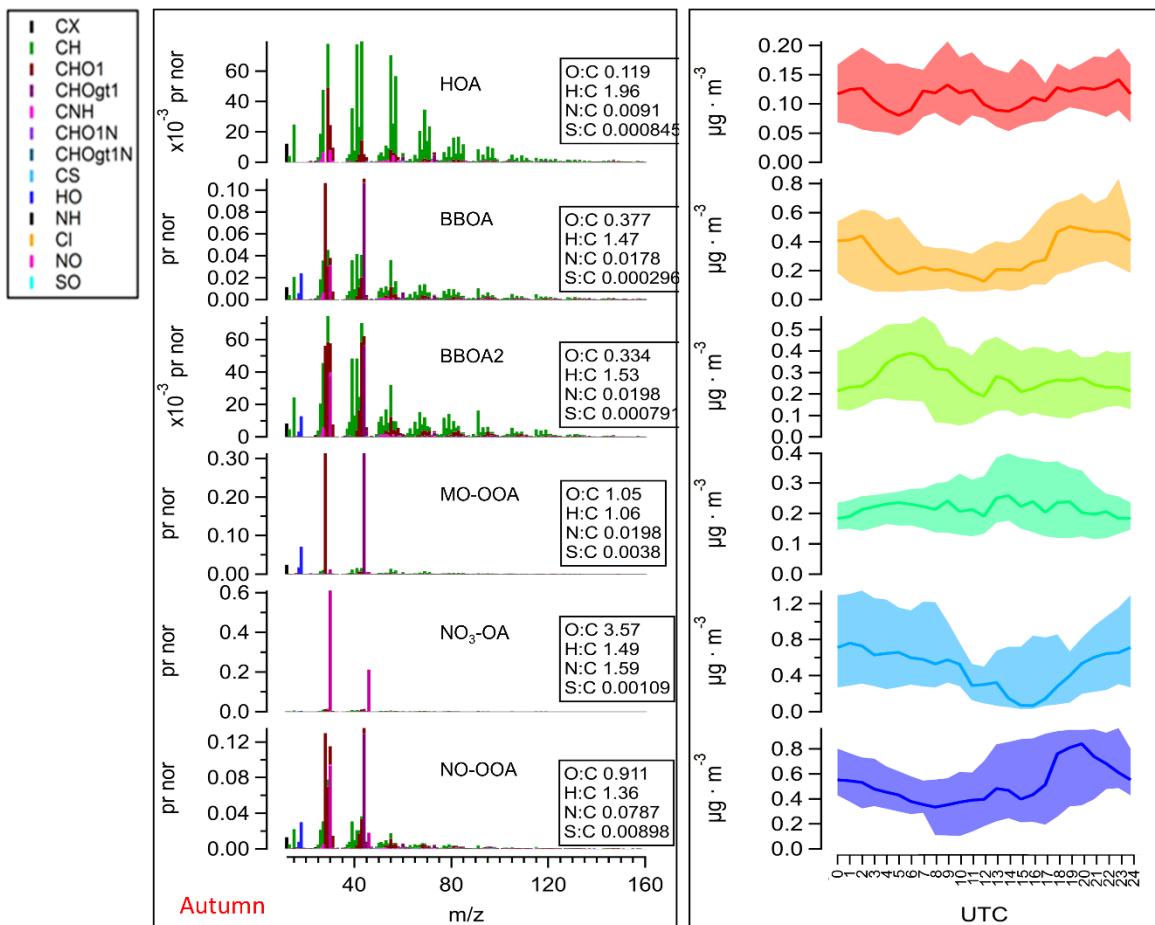
Figure S7 The results overview of source apportionment resolved by PMF analysis of aerosol nitrate and organics for the autumn of 2019. From left to right, the graph shows the variation of contribution to OA for each source factor, i.e. the high-resolution spectra of source factors colored by the family group of ions, and the diurnal pattern of the median (solid line) and interquartile range (IQR, shaded area) of the contribution of the corresponding source factor. The elemental ratio (OM:OC, O:C, H:C) of all OA factors is shown in the graph.
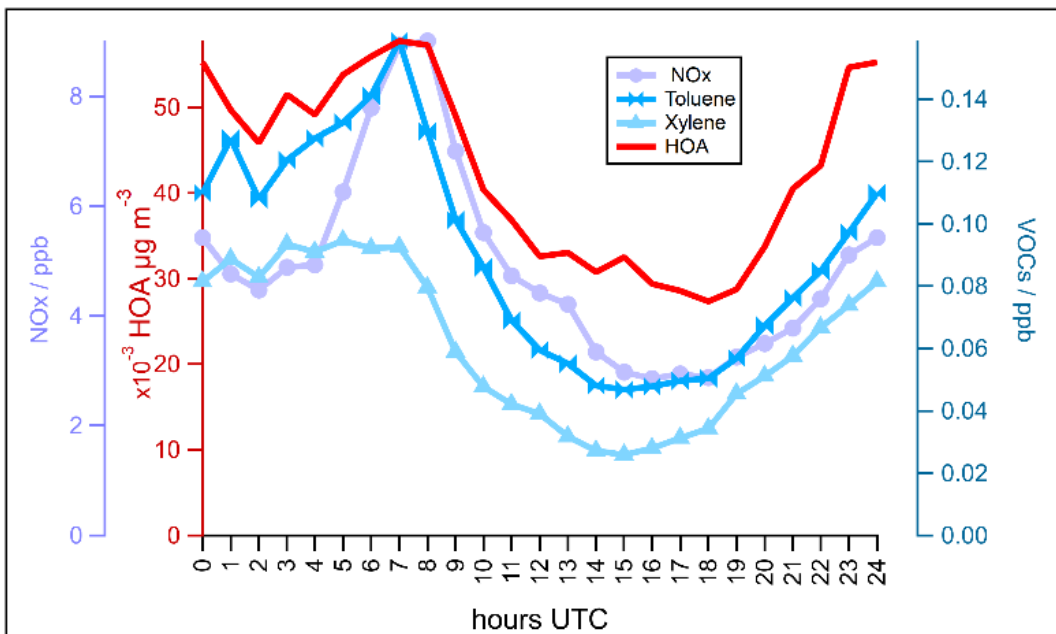
Figure S8 Comparison of the diurnal variation of the OA contribution of the HOA factor, the concentration of NOx, toluene, and xylene during the JULIAC-II. Toluene and Xylene use the same y-axis named VOC.
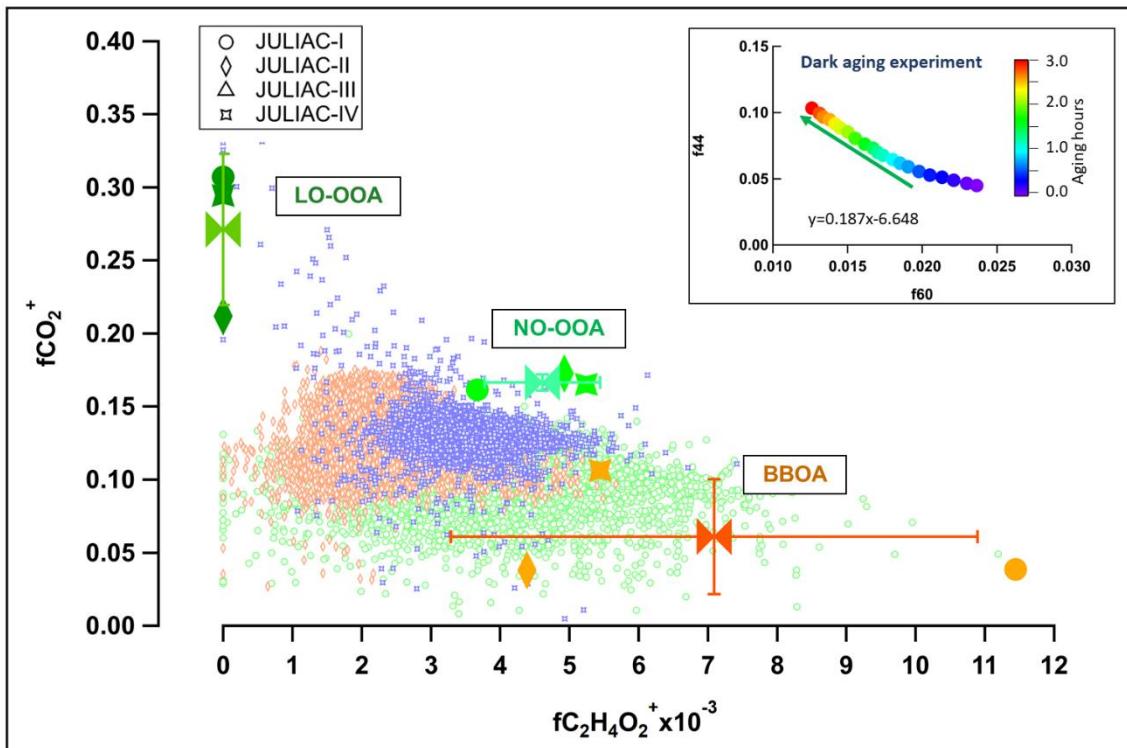
Figure S9 : fCO$_2^+$ (fraction of fragment CO$_2^+$ in OA) vs fC$_2$H$_4$O$_2^+$ (fraction of fragment C$_2$H$_4$O$_2^+$ in OA) for raw organic aerosols, and MO-OOA, NO-OOA, and BBOA factors' profile during the JULIAC-I, JULIAC-II, and JULIAC-IV are given. Means value and stand derivation error bar for these three types of source factors are also displaye. A small window at the upper right corner displays the evolution of HR-ToF-AMS measured OA through f60 vs f44 space for 3 hours' biomass burning dark aging laboratory experiments (Kodros et al., 2020).
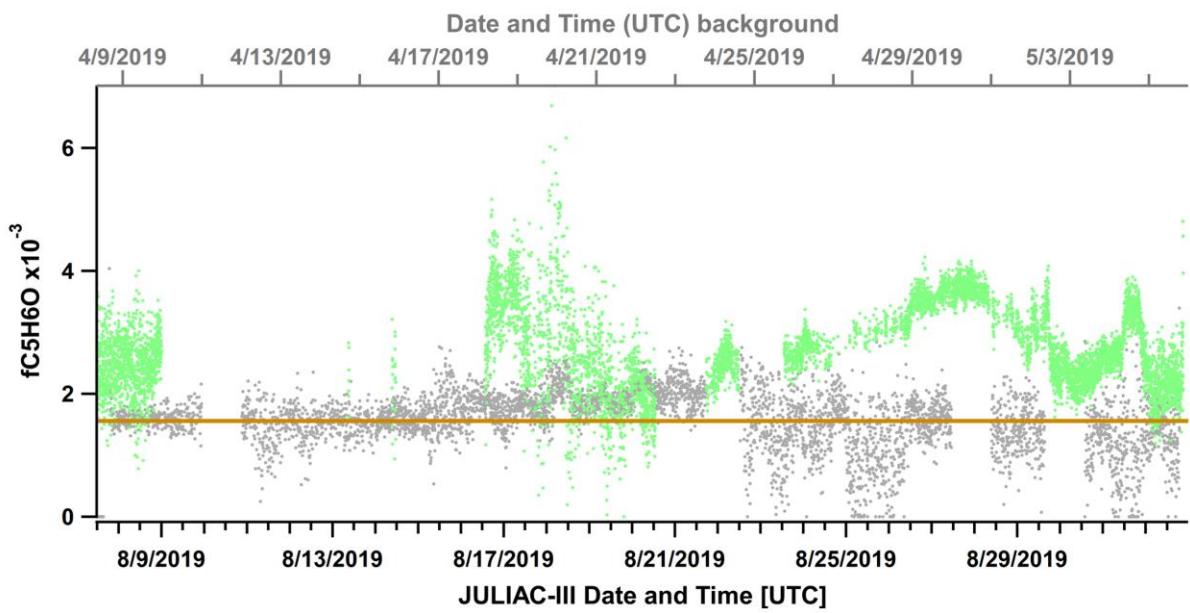
Figure S10 Comparison of fraction of ion fragment $C_5H_6O^+$ ($fC_5H_6O^+$) to total OA during the summer (JULIAC-III, bottom X-axis, green dot) and during the spring (JULIAC-II, top x-axis, grey dot). Here the grey dots aims to represent the background level of $fC_5H_6O^+$ when the seondary OA formation from biogenic emissions is not strong.
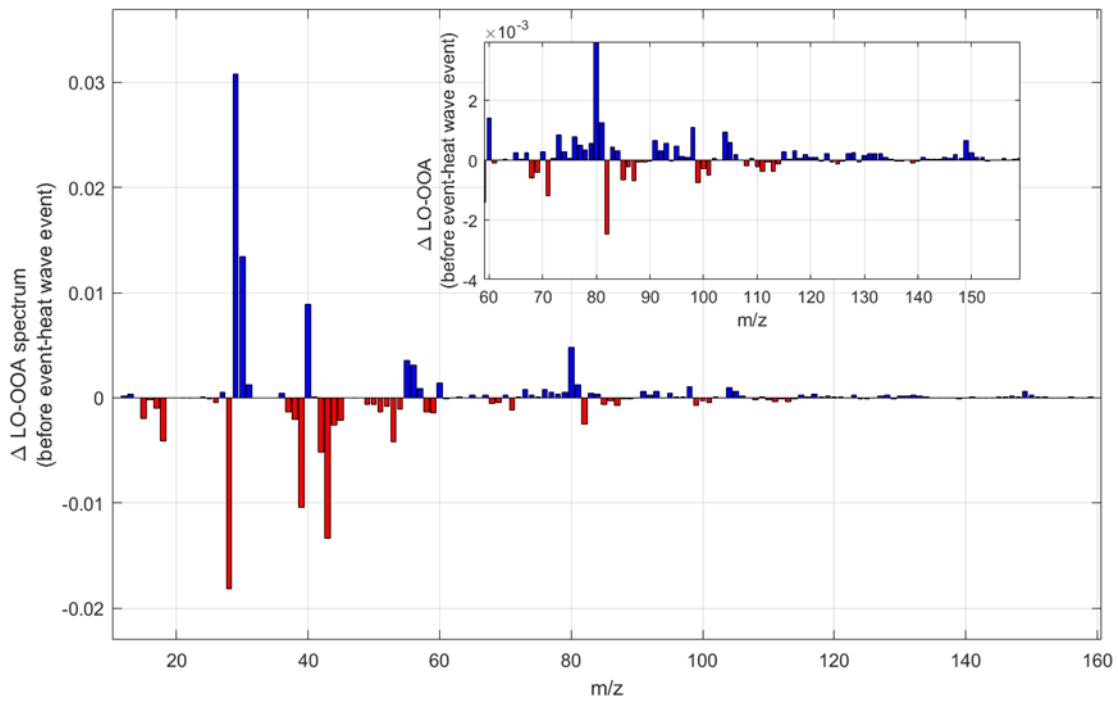
Figure S11 The difference in factor spectrum of LO-OOA source before and during the heat wave event. The y-axis represents the difference of mass fraction of organic signal at each mass-to-charge ratio (m/z) normalized to the total mass of OA. The insert window shows the detailed mass spectrum difference at regions of higher molecular weight with m/z>60. The blue color bar shows the ion peaks, which have a higher intensity before the heat wave event, while the red color bar represents the ions enhanced during the haze event

Table S1*:* The overview of the value of applied RIE_{NH4} and RIE_{SO4} for all four JULIAC intensive phases.

Phases	RIE_NH$_4$	RIE_SO$_4$
JULIAC-I	3.84	0.98
JULIAC-II	3.52	1.06
JULIAC-III	4.41	1.18
JULIAC-IV	3.84	1.18

Table S2*:* Composition of the VOC calibration standard used for PTR-ToF-MS calibration during the JULIAC campaigns, including nominal mixing ratios and associated uncertainties.

Substance	Mixing ratio [ppb]	Error [%]
Benzene	673.69	6.64
Toluene	671.46	6.47
a-Xylene	675.45	6.37
Mesitylene	670.71	6.3
Chlorbenzene	685.19	6.49
Acetaldehyde	632.64	7.58
Acetone	769.27	6.7
2-Butanone	671.63	6.64
3-Pentanone	683.85	6.45
MVK	669.75	6.7
Nopinone	668.2	6.3
alpha pinene	673.34	6.25
Isoprene	677.7	6.51
Methanol	677.18	8.45
1-Butanol	671.02	6.61
Acetonitrile	675.42	7.58

Table S3: Cross-correlation analysis (R^2 and theta angle) of HOA spectrum among seasonal HOA resolved in four JU-

LIAC phases and HOA factor reported in previous PMF studies (referred HOA factor data supported by high-resolution

AMS spectral database, <u>High Resolution AMS Spectral Database (colorado.edu)</u>). The background colors of coefficient

cell are color scales following the value of R^2.

R^2 / Theta	HOA_JULIAC-I	HOA_JULIAC-II	HOA_JULIAC-III	HOA_JULIAC-IV	Reference
U_DAURE_BCN_2009_HOA	0.81 / 23.71˚	0.99 / 12.80˚	0.98 / 12.80˚	0.72 / 33.08˚	(Mohr et al., 2012)
A_HR_031_HOA	0.82 / 23.93˚	0.83 / 24.02˚	0.82 / 24.02˚	0.82 / 24.34˚	(Crippa et al., 2013)
HOA_JULIAC-I	1.00 / 0˚	0.83 / 21.97˚	0.85 / 21.97˚	0.88 / 20.01˚	JULIAC-I
HOA_JULIAC-II	0.83 / 21.97˚	1.00 / 0˚	0.99 / 0˚	0.75 / 28.87˚	JULIAC-II
HOA_JULIAC-III	0.85 / 21.97˚	0.99 / 0˚	1.00 / 0˚	0.75 / 28.87˚	JULIAC-III
HOA_JULIAC-IV	0.88 / 20.01˚	0.75 / 28.87˚	0.75 / 28.87˚	1.00 / 0˚	JULIAC-IV

Table S4: Cross-correlation analysis (R^2 and theta angle) of BBOA spectrum among seasonal BBOA resolved in all four JULIAC phases and BBOA, CCOA factors reported in previous PMF studies (referred BBOA+CCOA factor data supported by high-resolution AMS spectral database, High Resolution AMS Spectral Database (colorado.edu)). The background colors of the coefficient cell are color scales following the value of R^2.

R^2 / Theta	BBOA JULIAC-I	BBOA JULIAC-II	BBOA JULIAC-IV	BBOA2 JULIAC-IV	Reference
U_DAURE_BCN_2009_BBOA	0.44 / 46.80°	0.79 / 34.73°	0.26 / 56.13°	0.59 / 40.61°	(Mohr et al., 2012)
A_HR_052_BBOA	0.84 / 22.74°	0.76 / 27.92°	0.82 / 24.58°	0.94 / 14.23°	(Hu et al., 2013)
A_HR_053_CCOA	0.64 / 34.92°	0.53 / 40.97°	0.92 / 16.23°	0.80 / 24.83°	(Hu et al., 2013)
BBOA_JULIAC-I	1.00 / 0°	0.58 / 38.87°	0.63 / 36.32°	0.76 / 28.17°	JULIAC-I
BBOA_JULIAC-II	0.58 / 38.87°	1.00 / 0°	0.49 / 43.83°	0.81 / 24.62°	JULIAC-II
BBOA_JULIAC-IV	0.63 / 36.32°	0.49 / 43.83°	1.00 / 0°	0.81 / 24.79°	JULIAC-IV
BBOA2_JULIAC-IV	0.76 / 28.17°	0.81 / 24.62°	0.81 / 24.79°	1.00 / 0°	JULIAC-IV

Table S5: Cross-correlation analysis (R^2 and theta angle) of OOA spectrum among seasonal OOA resolved in all four JULIAC phases and OOA factors reported in previous PMF studies (referred OOA factor data supported by high-resolution AMS spectral database, [High Resolution AMS Spectral Database (colorado.edu)](#)). The background colors of coefficient cell are color scales following the value of R^2.

R^2	MO-OOA _JULIAC-I	LO-OOA _JULIAC-II	LO-OOA _JULIAC-III	MO-OOA _JULIAC-IV	Reference
U_DAURE_BCN_2009_SV OOA	0.55 / 42.84°	0.64 / 37.43°	0.70 / 34.10°	0.57 / 42.11°	(Mohr et al., 2012)
A_HR_057_SV_OOA	0.88 / 20.62°	0.95 / 13.02°	0.97 / 9.43°	0.89 / 19.90°	(Hu et al., 2013)
A_HR_051_SVOOA_HR	0.63 / 37.46°	0.81 / 25.67°	0.85 / 23.89°	0.65 / 36.44°	(Hayes et al., 2013)
U_DAURE_BCN_2009_LV OOA	0.85 / 23.20°	0.92 / 17.59°	0.96 / 13.22°	0.85 / 22.99°	(Mohr et al., 2012)
A_HR_030_LV_OOA	0.82 / 26.12°	0.93 / 16.94°	0.97 / 12.49°	0.83 / 25.58°	(Crippa et al., 2013)
A_HR_050_LVOOA_HR	0.90 / 18.42°	0.98 / 7.70°	0.98 / 10.74°	0.91 / 17.84°	(Hayes et al., 2013)
A_HR_058_LV_OOA	0.93 / 15.72°	0.98 / 8.80°	0.99 / 5.90°	0.93 / 15.24°	(Hu et al., 2013)
A_HR_029_MOA	0.30 / 55.34°	0.38 / 49.96°	0.50 / 42.98°	0.31 / 54.95°	(Crippa et al., 2013)
A_HR_070_MO_OOA	0.85 / 22.93°	0.94 / 14.48°	0.97 / 10.03°	0.86 / 22.59°	(Hu et al., 2015)
A_HR_049_LOA_HR	0.59 / 39.76°	0.71 / 32.00°	0.74 / 30.65°	0.61 / 38.88°	(Hayes et al., 2013)
A_HR_071_LO_OOA	0.46 / 47.32°	0.63 / 36.66°	0.72 / 31.56°	0.47 / 46.57°	(Hu et al., 2015)
A_HR_072_LO_OOA	0.39 / 51.19°	0.58 / 39.88°	0.66 / 35.05°	0.40 / 50.35°	(Hu et al., 2015)
MO_OOA_JULIAC-I	1.00 / 0°	0.95 / 13.30°	0.91 / 17.82°	1.00 / 1.72°	JULIAC-I
LO_OOA_JULIAC-II	0.95 / 13.30°	1.00 / 0°	0.98 / 8.42°	0.95 / 12.53°	JULIAC-II
LO_OOA_JULIAC-III	0.91 / 17.82°	0.98 / 8.42°	1.00 / 0°	0.91 / 17.16°	JULIAC-III
MO_OOA_JULIAC-IV	1.00 / 1.72°	0.95 / 12.53°	0.91 / 17.16°	1.00 / 0°	JULIAC-IV

Table S6: The source factors and diagnostic parameters overview of the final selected optimal PMF run for all four JULIAC intensive phases. All source factors resolved in this study are displayed: Hydrocarbon-Like Organic Aerosol (HOA), Biomass Burning Organic Aerosol (BBOA), Less Oxidized Oxygenated Organic Aerosol (LO-OOA), More Oxidized Oxygenated Organic Aerosol (MO-OOA), Nocturnal Oxidation Oxygenated Organic Aerosol (NO-OOA), Methanesulfonic Acid-Containing Organic Aerosol (MSA-OA), Continental Regional Transport Organic Aerosol (Trans-OA).

JULIAC Phases	Q/Qexp	UEV (Unexplained noise+Unexplained real signals)	Resolved factors numbers	Resolved PMF factors
JULIAC-I	1.04	0.37 (0.29+0.08)	5	HOA, BBOA, Continental transport-OA, MO-OOA, NO-OOA
JULIAC-II	1.03	0.31 (0.22+0.09)	6	HOA, BBOA, Trans-OA, Marine transprot-OA, LO-OOA, NO-OOA
JULIAC-III	3.20	0.28 (0.14+0.14)	4	HOA, Marine transprot-OA,, LO-OOA, NO-OOA
JULIAC-IV	3.30	0.25 (0.11+0.14)	5	HOA, BBOA, BBOA2, MO-OOA, NO-OOA

Table S7: Overview of the averaged elemental ratio O:C, H:C, OS_C with corresponding standard variation of total organic aerosol for all four JULIAC intensive phases.

Averaged elemental ratio	JULIAC campaign			
	JULIAC-I/Winter	JULIAC-II/Spring	JULIAC-III/summer	JULIAC-IV/autumn
O:C	0.71±0.20	0.76±0.12	0.64±0.08	0.66±0.09
H:C	1.63±0.11	1.50±0.10	1.50±0.08	1.50±0.06
OSc	-0.21±0.41	0.01±0.26	-0.23±0.23	-0.18±0.23

Table S8: Correlation coefficient among the mass variation of biogenic-derived SOA (LO-OOA(Bio)), aerosol organo-

sulfur (OS), and aerosol bulk species (nitrate, sulfate and organics).

R	Aerosol volume conc from SMPS	Aerosol surface conc from SMPS	Aerosol number conc from SMPS
LO-OOA(Bio)	0.86	0.80	0.29
OS	0.84	0.80	0.33
$HRSO_4$	0.85	0.81	0.35
HROrg	0.86	0.82	0.37
$HRNO_3$	0.35	0.37	0.29

Reference

Crippa, M., El Haddad, I., Slowik, J. G., DeCarlo, P. F., Mohr, C., Heringa, M. F.,Prévôt, A. S. H.: Identification of marine and continental aerosol sources in Paris using high resolution aerosol mass spectrometry, Journal of Geophysical Research: Atmospheres, 118, 1950-1963, https://doi.org/10.1002/jgrd.50151, 2013.

Hayes, P. L., Ortega, A. M., Cubison, M. J., Froyd, K. D., Zhao, Y., Cliff, S. S.,Jimenez, J. L.: Organic aerosol composition and sources in Pasadena, California, during the 2010 CalNex campaign, Journal of Geophysical Research: Atmospheres, 118, 9233-9257, https://doi.org/10.1002/jgrd.50530, 2013.

Hu, W. W., Hu, M., Yuan, B., Jimenez, J. L., Tang, Q., Peng, J. F.,He, L. Y.: Insights on organic aerosol aging and the influence of coal combustion at a regional receptor site of central eastern China, Atmos. Chem. Phys., 13, 10095-10112, https://doi.org/10.5194/acp-13-10095-2013, 2013.

Hu, W. W., Campuzano-Jost, P., Palm, B. B., Day, D. A., Ortega, A. M., Hayes, P. L.,Jimenez, J. L.: Characterization of a real-time tracer for isoprene epoxydiols-derived secondary organic aerosol (IEPOX-SOA) from aerosol mass spectrometer measurements, Atmos Chem Phys, 15, 11807-11833, https://doi.org/10.5194/acp-15-11807-2015, 2015.

Kodros, J. K., Papanastasiou, D. K., Paglione, M., Masiol, M., Squizzato, S., Florou, K.,Pandis, S. N.: Rapid dark aging of biomass burning as an overlooked source of oxidized organic aerosol, Proc Natl Acad Sci U S A, 117, 33028-33033, https://doi.org/10.1073/pnas.2010365117, 2020.

Mohr, C., DeCarlo, P. F., Heringa, M. F., Chirico, R., Slowik, J. G., Richter, R.,Prévôt, A. S. H.: Identification and quantification of organic aerosol from cooking and other sources in Barcelona using aerosol mass spectrometer data, Atmos Chem Phys, 12, 1649-1665, https://doi.org/10.5194/acp-12-1649-2012, 2012.